Available online at www.CivileJournal.org

Civil Engineering Journal

(E-ISSN: 2476-3055; ISSN: 2676-6957)

Vol. 9, No. 01, January, 2023

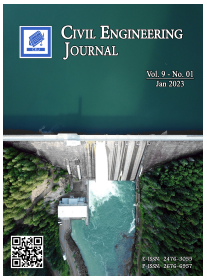

The Influence of Moisture on the Frequency Spectrum of Time Varying Mass Engineering Structure

Phung Tu [1*], Vanissorn Vimonsatit [2], Chayanon Hansapinyo [3]

[1] *Flow without Quake, Perth, Western Australia 6000, Australia.*

[2] *School of Engineering, Macquarie University, Sydney, 2113, NSW, Australia.*

[3] *Excellence Center in Infrastructure Technology and Transportation Engineering, Department of Civil Engineering, Chiang Mai University, Chiang Mai, 50200, Thailand.*

Received 11 October 2022; Revised 07 December 2022; Accepted 18 December 2022; Published 01 January 2023

Abstract

The frequencies of time-varying mass systems have not been commonly studied in engineering structures as the rate of mass change is generally small compared to the mass of the overall structure. For silos of granular materials, the total mass of the stored granules can be relatively high compared to the mass of the silo structure. During the flow-in or flow-out of granules, the silo system behaves as a time-varying mass system. Minor changes to the moisture content ratio of the granules can cause their flow characteristics to change. The influence of the moisture content ratio of the granular material inside a cylindrical silo is investigated in this paper using Variational Mode Decomposition, Hilbert Transform, and Hilbert Marginal Spectrum processing methods. The results show that the amplitude and frequency of vibration vary with the change in the moisture content ratio of the stored materials and across different cycles, despite all influencing parameters being kept constant. Such variations in the response of the structure mean that the loads also vary according to the principles of engineering mechanics. The outcomes of this research can be further developed into a diagnostic tool to conditionally monitor the structural integrity of the overall silo structure and flow characteristics automatically.

Keywords: HMS; VMF; VMD; HT; Frequency Spectrum; Time Varying Mass Civil Engineering Structure; Moisture Content Ratio.

1. Introduction

In mechanics, a variable-mass system consists of matter whose mass varies significantly over time. In such cases, the effects of the varying mass and the momentum of the mass exiting or entering the system need to be accounted for. The term "time-varying mass" (TVM) often refers to branches of science such as planetary motions and rockets. In reality, the overall mass of an engineering structure varies with time, though in most cases, an engineering structure is not considered a time varying mass dynamic system because the rate of change of the total mass is rather gradual. As such, the dynamic effects of the mass loss are insignificant and often can be accounted for by the inclusion of a dynamic load factor in the static analysis. However, in structures used to store bulk materials, such as a silo, where the rate of change of the total mass is significant, particularly when the weight ratio between the stored materials and the structure is high, the mass in contact with the structure is unrestrained and has varying mechanical properties. In such cases, the motions of the overall system (structure and stored materials leaving or exiting the storage structure) can influence the interactions between the granular particles stored inside the structure and the structure. Such interactions can amplify the forces between the granular particles and the structure beyond the load resistance capacity of the structure and cause other integrity issues, such as resonance, cracking of the structure, and catastrophic failures.

* Corresponding author: phung.tu@flowwithoutquake.com

http://dx.doi.org/10.28991/CEJ-2023-09-01-02

In silo operations, it is in the best interest of the operator to empty and refill the silo as quickly as possible to maximize production throughput. In all cases, the granular particles inside the silo are unrestrained, differ in size and shape [1], and the moisture content ratio [2] can vary between seasons, especially if the stockpile is subjected to the weather. To our knowledge, how particle size, shape, and moisture content ratio dynamically interact with the overall silo structure has not been studied in detail because the silo structure has always been assumed to be infinitely rigid as suggested by the fundamental silo load theory, Janssen's silo theory, formulated in 1895. In reality, every structure has a finite stiffness, and as such, there is a need to understand and quantify such complex interactions between the mass of the content in contact with the structure and the structure itself. Also, it is very concerning that according to Janssen's silo load theory, the fundamental theory of silo engineering, the walls of the silo cave inward and the granular particles inside the silo spill out the top of the silo when it is filled, as suggested in Figure 1 [3] and the subsequent Equations 1 to 5.

$$\sigma_v(z) + g\rho_b A dz - \tau_w(z) - \sigma_v(z+dz) = 0 \quad (1)$$

$$\sigma_v(z) + g\rho_b A dz - \tau_w(z) - \sigma_v(z) - \sigma_v(d_z) = 0 \quad (2)$$

$$g\rho_b A dz - \tau_w(z) - \sigma_v(d_z) = 0 \quad (3)$$

$$g\rho_b A dz = \tau_w(z) + \sigma_v(d_z) \quad (4)$$

$$g\rho_b A dz = K\tan(\varphi_x)\sigma_v(z) + \sigma_v(d_z) \quad (5)$$

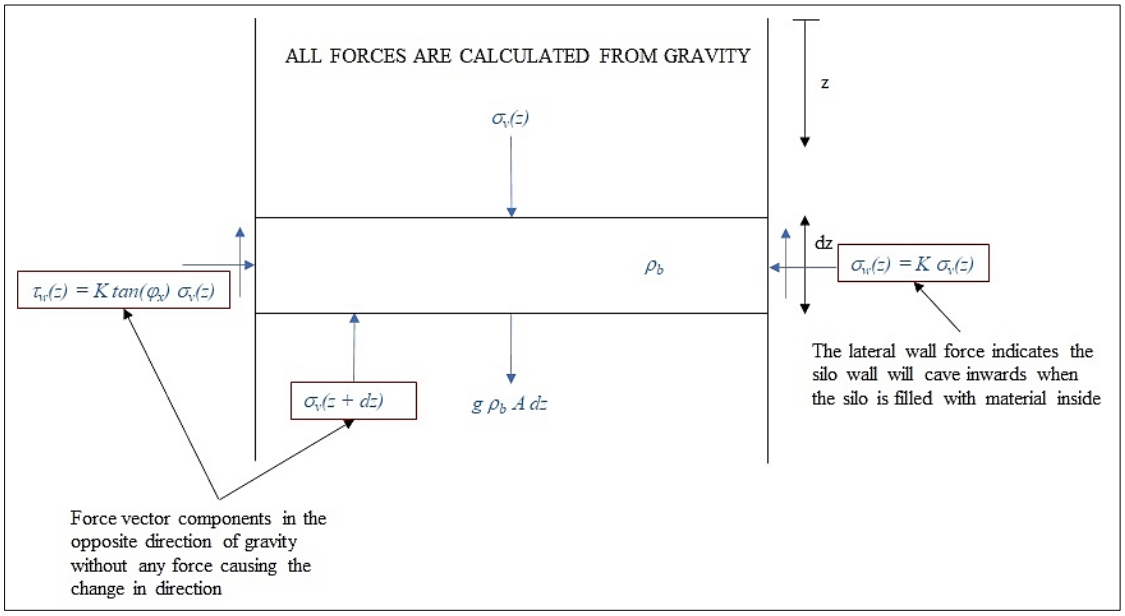

Figure 1. Janssen's silo load theory

The force equilibrium is expressed in Equation 1. It is often found in the literature on silo loadings that Equation 1 is integrated mathematically without further simplification. However, if one were to use simple algebra to evaluate and simplify Equation 1 further, one would find that Equation 1 is reduced to Equation 5.

In these equations, z is the depth from the top of the column of material inside the silo, A is the cross sectional area of the horizontal slice, ρ_b is the bulk density of the granular material, g is the gravity, φ_x is the friction angle between the wall and the material, $\sigma_v(z)$ is the vertical force at the upper face at depth z. Thus, $g\rho_b A dz$ represents the weight of the elemental slice dz, and K is the lateral pressure coefficient that determines the magnitude of the force $\sigma_v(z)$ acting perpendicular to the wall of the silo, where $\sigma_w(z) = K\sigma_v(z)$. K has a range between zero and one, with zero when there is no distribution of the vertical force to the wall, and one means all of the vertical force is distributed to the wall and nothing distributed to the material layer under the horizontal slice of interest.

The term $\tau_w(z)$ is the traction force on the wall in the opposite direction to the applied force $\sigma_v(z)$ where $\tau_w(z) = K\tan(\varphi_x)\sigma_v(z)$, and $\sigma_v(z+dz)$ is the reaction force beneath the elemental slice, suggesting there is no distribution of the weight of the elemental slice to the wall, that is $\tau_w(z) = K\tan(\varphi_x)\sigma_v(z)$, not $\tau_w(z) = K\tan(\varphi_x)\sigma_v(z+dz)$.

It is very clear in Equation 5 that there is an imbalance force $K\tan(\varphi_x)\sigma_v(z)$ with a direction upwards unless the product of $K\tan(\varphi_x)\sigma_v(z)$ is zero. In such cases, either K or $\tan(\varphi_x)$ needs to be zero. Furthermore, when $K\tan(\varphi_x)\sigma_v(z)$ is zero, the bulk solid behaves like a liquid. According to Newton's first law of motion, this imbalance force will cause the material column to move upwards and spill out the top of the silo when it is filled. Furthermore, when Newton's first law of motion is used to assess the stability of the walls of the silo in Janssen's silo theory, it can be found that the walls cave inwards when the silo is filled because there is no force to resist the walls from moving and

those forces ($\sigma_w(z)$) only cancel each other once the walls on either side of the horizontal slice are in contact with each other.

The technical flaws in the fundamental silo load theory have resulted in the frequencies generated during discharge not getting the deserved attention. This is evident in a publication by Xu & Liang (2022) [4]. Figure 4 produced by Xu & Liang (2022) [4], shows the experimental pressures fluctuating throughout the entire duration of the discharge process. However, Xu & Liang (2022) [4] provided no explanations on how those fluctuating pressures were converted to match their theory and how the frequencies were incorporated. The study of the frequency spectrum using nonlinear and nonstationary signal processing techniques was first proposed by Tu (2017) [5] and, Tu et al., (2018) [6] to study the frequencies generated by a discharging silo. In a later study, Tu et al. (2022) [7] investigated the frequency spectrum of a time varying mass structure using a combination of advanced signal processing techniques such as Variational Mode Decomposition (VMD), Hilbert Transform (HT), and Hilbert Marginal Spectrum (HMS). Tu et al. (2022) [7] reported differences in the frequencies generated by a steel silo with iron ore compared to a perspex tube filled with sand. It was also found that different areas on the silo produce different dominant frequencies. The study of the frequencies of the overall structure is common in the fields of structural dynamics and earthquake engineering. In fact, international structural loading standards such as AS/NZS1170.4 (2007) [8] and AS2304 (2019) [9] have provisions to incorporate the time varying frequencies of the imposed actions and the natural frequencies of the overall structure into the design of the structure for safety reasons.

In this paper, Variational Mode Decomposition (VMD) is used to decompose signals generated from a tube supported on a steel frame filled with sand of different moisture content ratios into a series of Variational Mode Functions (VMF). The Hilbert Transform (HT) is used to find instantaneous frequencies in the VMFs, and finally, the Hilbert Marginal Spectrum (HMS) is used to plot the total amplitude per frequency. It is well established in the field of structural dynamics that any vibration problem can be solved in the time domain or frequency domain. As such, the frequency spectrum can be developed into silo analysis and design methods similar to those found in earthquake engineering design standards, and methods to design the flow of the granular particles. In a separate study, Asencio et al. (2017) [10] demonstrated how 25000 cubes inside a container rearranged themselves into perfect order by applying torsional vibrations to the container. As such, it can be hypothesized that granular-structure interaction can promote and impede the flow of bulk material inside a container, thus warranting further attention. This study leads to a better understanding of the bidirectional interaction between the granular material and the structure, thus enabling the development of better analysis and design methods to optimize the silo in the design, better maintain and operate silos, and ultimately leading to improved safety and reductions in capital and operational expenditures. Furthermore, similar to techniques that have been developed to monitor the structural integrity of bridges, buildings, and machines, the frequency spectrum can be further developed to conditionally monitor the structural integrity of the silo and flow characteristics in real time without the need to take the silo out of service.

1.1. Signal Processing Theories

Dragomiretskiy & Zosso (2014) [11] introduced Variational Mode Decomposition (VMD) to decompose a signal f into a discrete number of sub-signals μ_k that have specific sparsity properties while reproducing the input. They assumed that each mode k is compact around a centre pulsation ω_k, which is determined along with the decomposition. The bandwidth of each mode is assessed by computing the associated analytic signal by means of the Hilbert Transform in order to obtain a unilateral frequency spectrum for each mode μ_k. The obtained frequency spectrum of each mode is shifted to the 'baseband' by mixing with an exponential tune to the respective estimated centre frequency. Finally, the bandwidth is estimated through the H^1 Gaussian smoothness of the demodulated signal (the squared L^2-norm of the gradient), resulting in a constrained variational problem shown in Equation 6.

$$\min_{\{u_k\},\{\omega_k\}} \left\{ \sum_k \left\| \partial_t \left[\left(\delta(t) + \frac{j}{\pi t} \right) * u_k(t) \right] e^{-j\omega_k t} \right\|_2^2 \right\} \quad \text{s.t. } \sum_k u_k = f \tag{6}$$

where $\{u_k\} := \{u_1, \dots, u_K\}$ is the shorthand notation for the set of all modes, $\{\omega_k\} := \{\omega_k, \dots, \omega_K\}$ represents the notation for the set of all centre frequencies, and $\sum_k := \sum_k^K$ is the summation of all the modes together.

Quadratic penalty terms and Lagrangian multipliers, λ, are introduced to remove reconstruction constraints. The quadratic penalty is a classic way to encourage reconstruction fidelity, typically in the presence of additive Independent and Identically Distributed (iid) Gaussian noise. The weight of the penalty term is derived from an inversely proportional Bayesian prior to the noise level in the data. The weight needs to be infinitely big in order to enforce strict data fidelity in a noise free setting, thus rendering the system ill-conditioned in the process. Lagrangian multipliers, on the other hand, are commonly added to enforce strict constraints. Combining quadratic terms and Lagrangian multipliers results in nice convergence properties of the quadratic penalty at finite weight, and produces the strict enforcement of the constraint by the Lagrangian multiplier. The complete algorithm is as follows:

- Initialise $\{\hat{u}_k^1\}, \{\omega_k^1\}, \hat{\lambda}^1, n \leftarrow 0$;
- Update the values according to the following formulae:

$$\hat{u}_k^{n+1} \leftarrow \frac{\hat{f}(\omega)-\sum_{i<k}\hat{u}_i^{n+1}(\omega)-\sum_{i>k}\hat{u}_i^{n}(\omega)+\frac{\hat{\lambda}^n(\omega)}{2}}{1+2\alpha(\omega-\omega_k^n)^2} \quad (7)$$

$$\omega_k^{n+1} \leftarrow \frac{\int_0^{+\infty}\omega|\hat{u}_k^{n+1}(\omega)|^2 d\omega}{\int_0^{+\infty}|\hat{u}_k^{n+1}(\omega)|^2 d\omega} \quad (8)$$

$$\hat{\lambda}^{n+1}(\omega) \leftarrow \hat{\lambda}^n(\omega) + \tau\left[\hat{f}(\omega) - \sum_k \hat{u}_k^{n+1}(\omega)\right] \quad (9)$$

- Repeat Equation 7 until the convergence criterion is satisfied Equation 10.

$$\sum_k \frac{\|\hat{u}_k^{n+1}-\hat{u}_k^n\|_2^2}{\|\hat{u}_k^n\|_2^2} < \epsilon \quad (10)$$

It was noted by Isham et al. (2018) [12] that the performance of VMD is dependent on a predetermined number of modes. An inaccurate number of modes will result in over and under decomposition that will affect the Variation Mode Functions (VMFs).

Hilbert Transform (HT) was introduced by David Hilbert to provide a mechanism to determine the instantaneous frequency and amplitude of a signal. The HT of a signal *c(s)* is defined as the transform in which the phase angle of all components of the signal is shifted by 90°. In Hilbert Huang Transform (HHT), HT is applied to the IMFs obtained from the EMD algorithm. In this paper, HT is applied to the VMFs from the VMD algorithm above to determine the instantaneous frequency and amplitude of a signal.

The Hilbert Transform $c_H(t)$ of any signal *c(s)* is defined as:

$$c_H(t) = \frac{1}{\pi} P \int_{-\infty}^{\infty} \frac{c(s)}{t-s} ds \quad (11)$$

$$z(t) = c(s) + jc_H(t) = a(t)e^{j\emptyset(t)} \quad (12)$$

$$a(t) = \sqrt{c(s)^2 + c_H(t)^2} \quad (13)$$

$$\emptyset(t) = \tan^{-1}\frac{c_H(t)}{c(s)} \quad (14)$$

$$w(t) = \frac{d\emptyset(t)}{dt} \quad (15)$$

where *P* is the Cauchy principal value of the singular integral, *c(s)* is the signal, $c_H(t)$ is the Hilbert transform of the original signal, *a(t)* is the amplitude of pre-envelope, and $\phi(t)$ is the instantaneous phase. The instantaneous frequencies are found by applying Equation 15. The original signal is expressed by applying Equation 16 where *R* is the real component of the Hilbert transform.

$$H(w,t) = R\sum_{i=1}^{n} a_i(t)\, exp(j\int w_i(t)dt) \quad (16)$$

$$h(w) = \int_0^T H(w,t)dt \quad (17)$$

With the Hilbert Spectrum defined, the Hilbert Marginal Spectrum (HMS) can be found by applying (17). The HMS represents a measure of the total amplitude or energy contribution from each frequency. The complete process is shown in Figure 2.

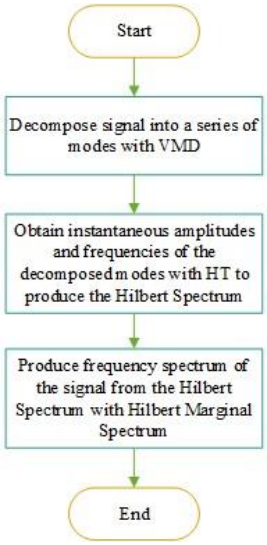

Figure 2. Flow chart showing the complete process of generating the frequency spectrum

2. Experimental Setup

The experiments conducted by Griffiths (2018) [13] were purposely designed to reproduce the honking phenomenon. In Griffiths' experiments, a polycarbonate hollow tube of 2000mm in length, 194 mm internal diameter and 3mm wall thickness was used. The tube rests on a welded steel frame with a plate at the top. Each plate was drilled with a hole in the middle to serve as an outlet. Outlet diameters of 60 mm, 90 mm, 120 mm, 150 mm, and 194 mm were selected to vary the discharge rates. In total, eight accelerometers (PCB Model 393B04) were screwed to the outside of the silo wall at 200 mm spacings starting 100 mm from the top of the silo (Figure 3). The accelerometers have a measurement range of plus or minus ±49 m/s² and a frequency range between 0.06 and 450 Hz. All accelerometers were connected to a QuantumX MX840B data logger, and the sampling rate of 1200 Hz was adopted.

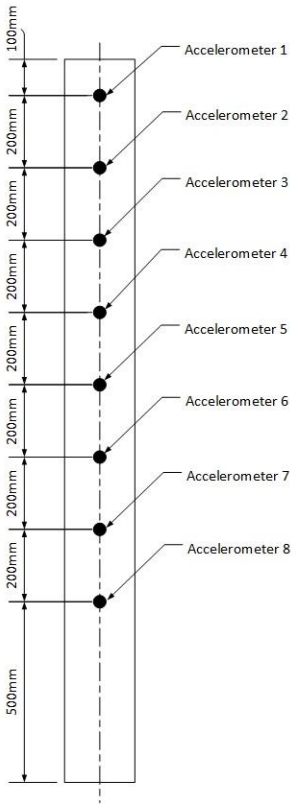

Figure 3. Locations of accelerometers mounted on the tube similar to the experimental setup

Figure 4. Locations of accelerometers mounted on the tube

Sand with a grain diameter of 300-600 µm was chosen to be the fill material for the experiment because it has repeatedly and reliably induced the vibration and booming sound. The sand particle size of 300-600 µm was selected as it fell within the range of most previous studies. The sand was dried and sieved utilising the multilevel sieve following the procedures set out in AS1289.3.6.1 (2009) [14]. However, only 300-600 µm sand particles were retained. The sand was thoroughly washed in distilled water until sufficient clarity was observed in the wash water to minimise the effect of contaminants in the material. A manageable amount of sand was poured into a bin and filled with water. The sand was then agitated by hand to pull any powders and impurities into the water column. The dirty water was then removed and refilled with clean water. This process was repeated until sufficient clarity in the agitated water column was achieved. It was impractical to place all 100kg of sand in the oven; thus, the cleaned sand was spread in drying trays and allowed to dry indoors for five days. After five days, the initially washed sand still had a residual moisture content of 1.6%. Griffiths (2018) [13] varied the moisture content of the sand spraying water to the 100kg sample. The sand was saturated with a spray bottle one kg at a time and transferred to a second bin. As each layer of sand was added to the bin, it was turned and mixed with the previous layer. Once all water was added, the entire sand sample was spread on a tarp and mixed further by hand to ensure uniform moisture distribution. The sand was then returned to its storage bin and allowed to stand for one hour to encourage even moisture distribution. Three samples of each prepared batch of sand were collected to be analysed following AS1289.2.1.1 (2005) [15] to determine the true achieved moisture content and confirm even moisture content distribution.

The sand with 1.6% moisture content was discharged through outlet diameters of 60 mm, 90 mm, 120 mm, 150 mm, and 194 mm. However, the sand with an average moisture content of 7.8% was discharged through only the 150 mm outlet diameter because outlet diameters below 150 mm caused blockages, and time was limited, so the outlet diameter of 194 mm was not used. The acceleration responses were denoised using wavelet algorithms and decomposed with VMD, outlined in Section 2, into their underlying VMFs and transformed using HT as shown in Equation 6 to obtain the instantaneous frequencies and amplitudes at the locations with accelerometers installed. The VMD and HT algorithms were provided by *MATLAB (R2022a)* edition. For the purpose of this paper, data collected from a 150 mm outlet for moisture content ratios of 1.6% and 7.8% were analysed and compared.

3. Results and Discussion

The denoised accelerations for sands with 1.6% and 7.8% moisture content ratios are reported in Figures 5 and 6, respectively. Griffiths (2018) [13] reported that loud foghorn sounds were heard during the experiments, and the increase in the moisture content ratio produced longer duration sound. From the physics of acoustics, vibrations of air molecules of frequencies between 20 Hz and 20000 Hz are within the human audible spectrum; thus, the sound heard would be expected to have frequencies within the human audible spectrum.

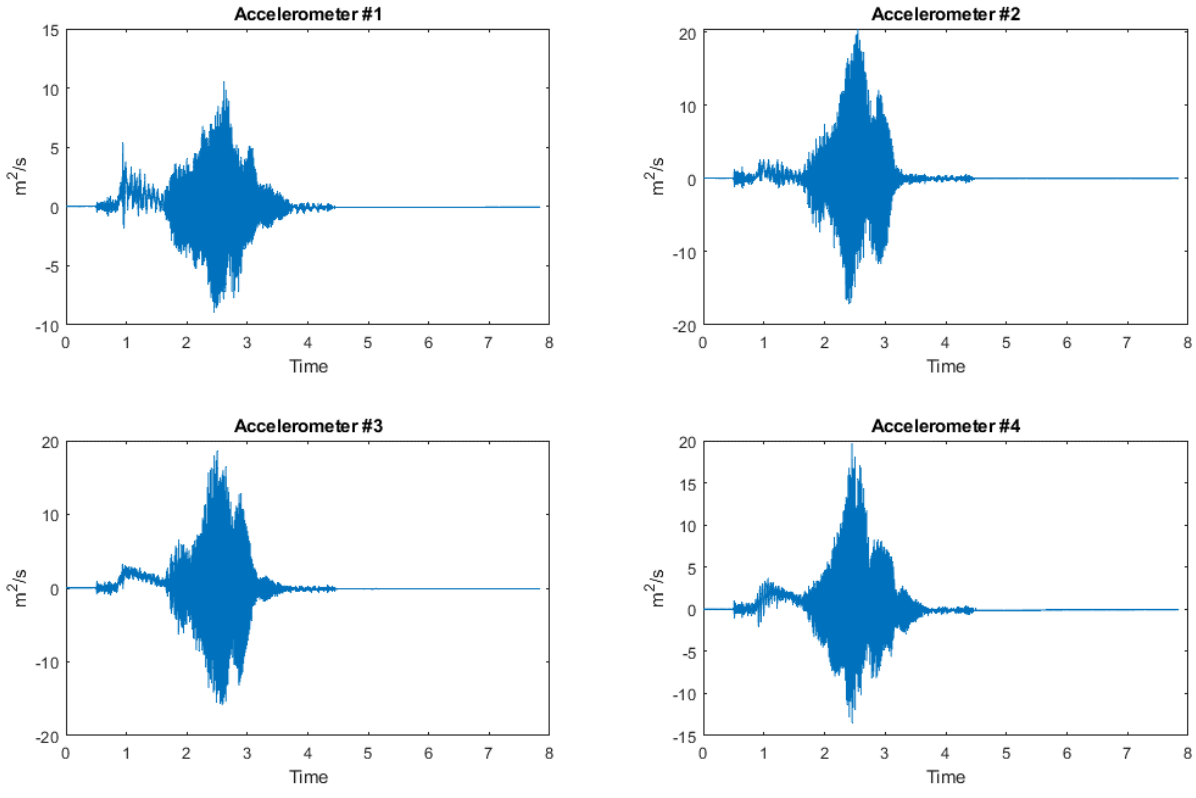

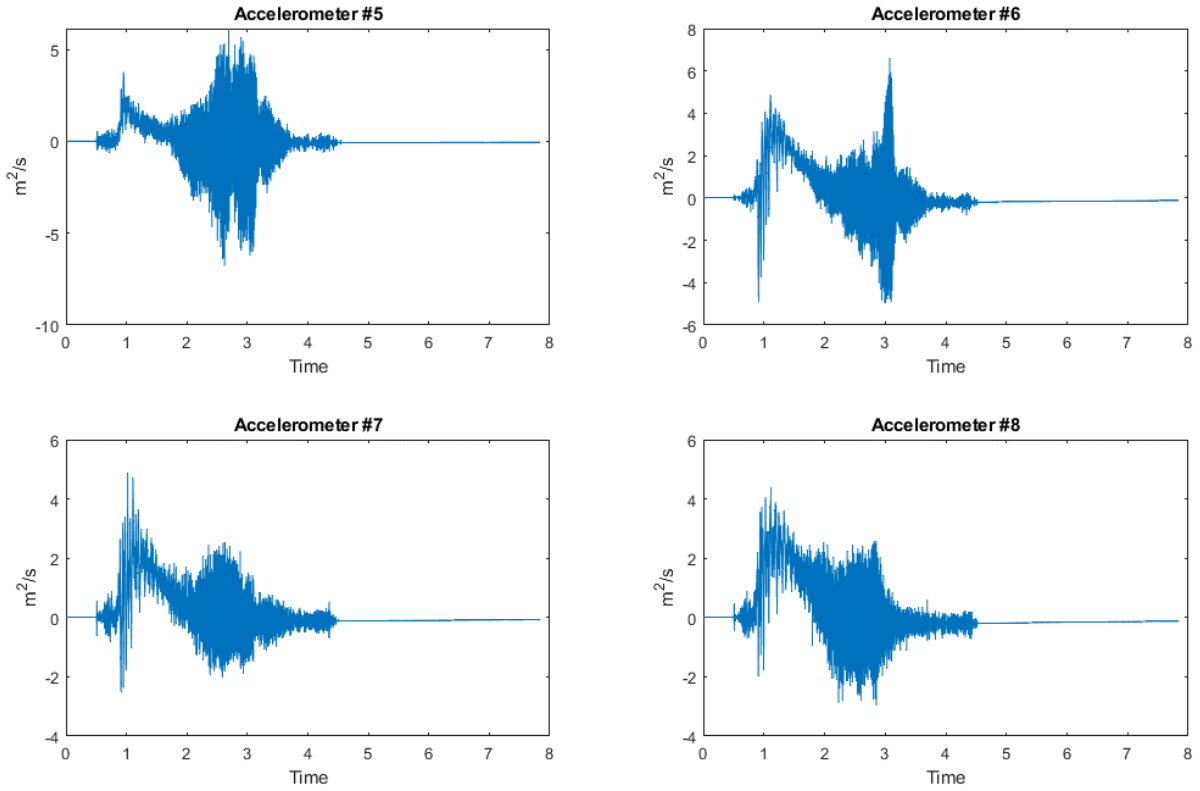

Figure 5. Accelerations for sand with 1.6% moisture content – 150 mm outlet diameter

The accelerometers used in the experiments could only sense vibrations between 0.6 Hz and 450 Hz. As such, the accelerometers could only sense a fraction of the frequencies produced. This is evident in Figures 5 and 6, where the accelerograms show upwards curves, above 0 m/s^2, in the first few seconds of the recordings. It is expected that accelerometers that can sense frequencies up to 20000 Hz would reveal more artifacts.

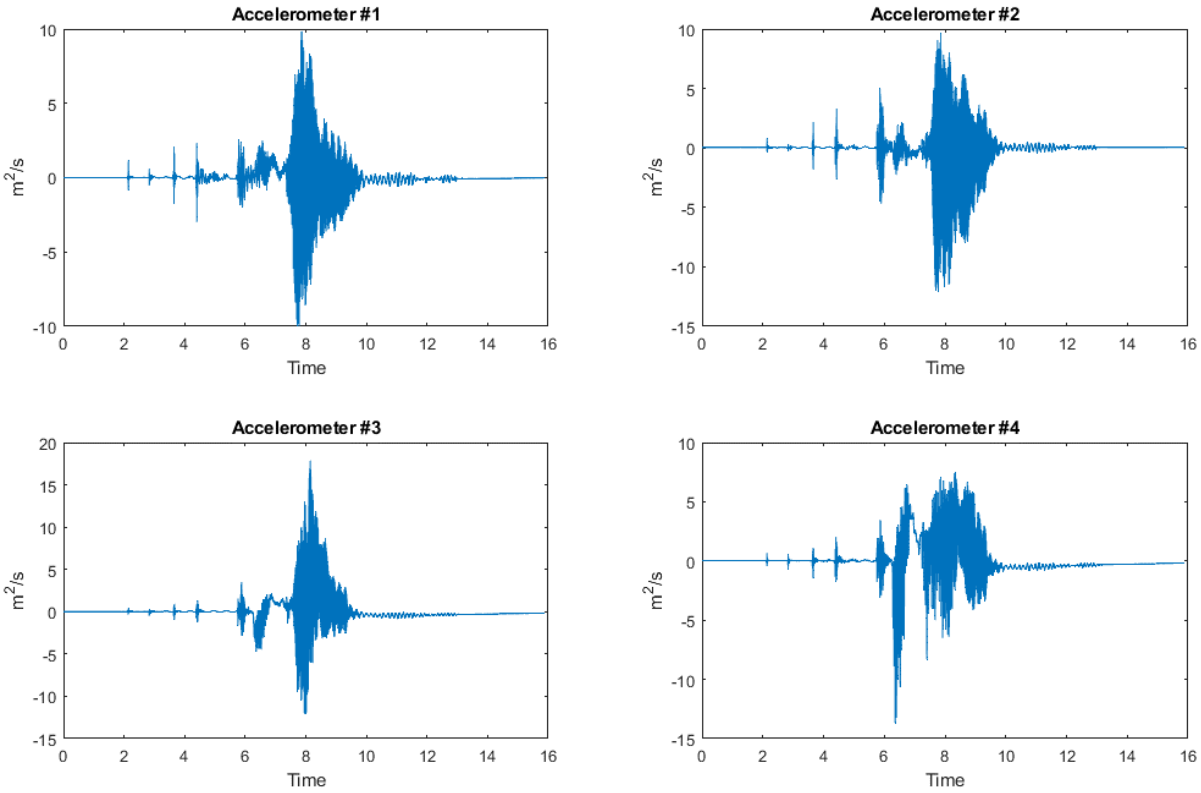

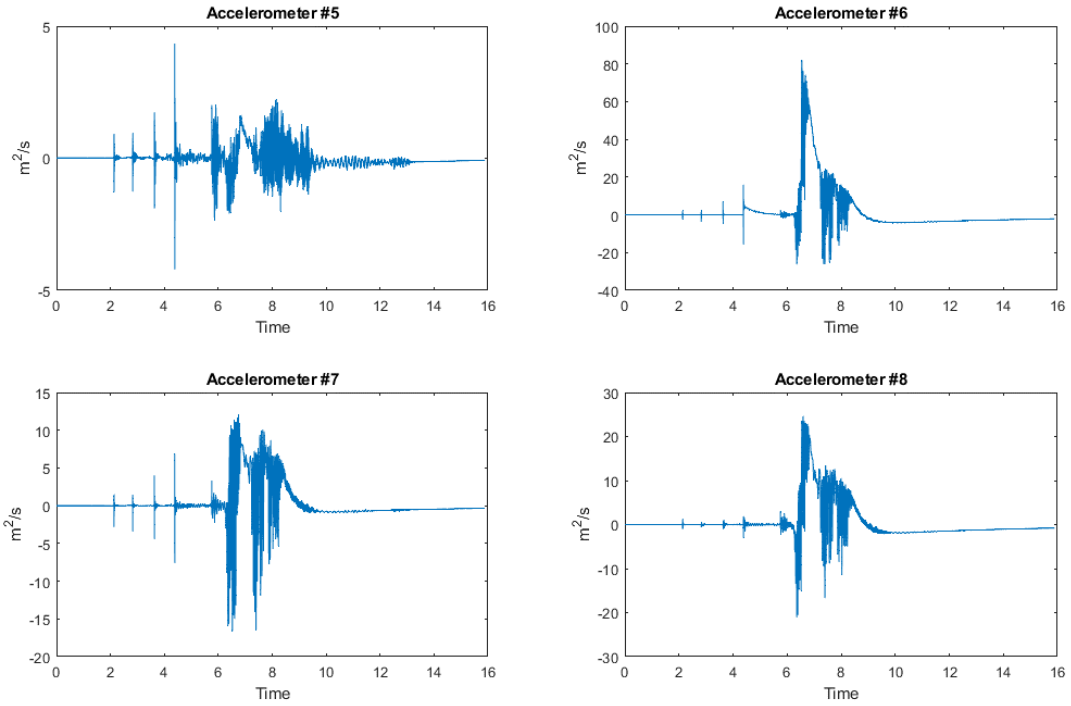

Figure 6. Accelerations for sand with 7.8% moisture content – 150 mm outlet diameter

The signals reveal differences in the frequency spectra between samples with 1.6% and 7.8% moisture content ratios (Figure 7). Accelerometer number 1 recorded similar response spectra with a 1.6% moisture content ratio and dominant frequencies around 1 Hz, 124 Hz and 265 Hz similar to the dominant frequencies of the sample with a 7.8% moisture content ratio. Accelerometer number 2 recorded the sample with a 7.8% moisture content ratio having dominant frequencies of about 62 Hz, 191 Hz, 202 Hz, and 253 Hz – different from the dominating frequencies of below 40Hz, and 193 Hz in the sample with a 1.6% moisture content ratio. The frequencies recorded by Accelerometer 3 are similar between the two samples; the sample with a moisture content ratio of 7.8% has dominant frequencies of 17 Hz, 192 Hz and 258 Hz; and the sample with a moisture content ratio of 1.6% has dominant frequencies of 1 Hz, 43 Hz, 189 Hz, and 265 Hz. The frequency spectra for Accelerometers 4, 6, 7 and 8 show remarkable differences between the two samples. Frequencies of 23 Hz, and 201 Hz stood out in the spectra for Accelerometer 4, 9 Hz stood out in the spectra for Accelerometer 6, 22 Hz in the spectra for Accelerometer 7 and 23 Hz for Accelerometer 8 in the sample with a moisture content ratio of 7.8%. Accelerometer 5 recorded frequencies of 122 Hz and 261 Hz in the sample with a 1.6% moisture content ratio. The change in the moisture content ratio causes differences in the frequency and amplitude along the height of the tube.

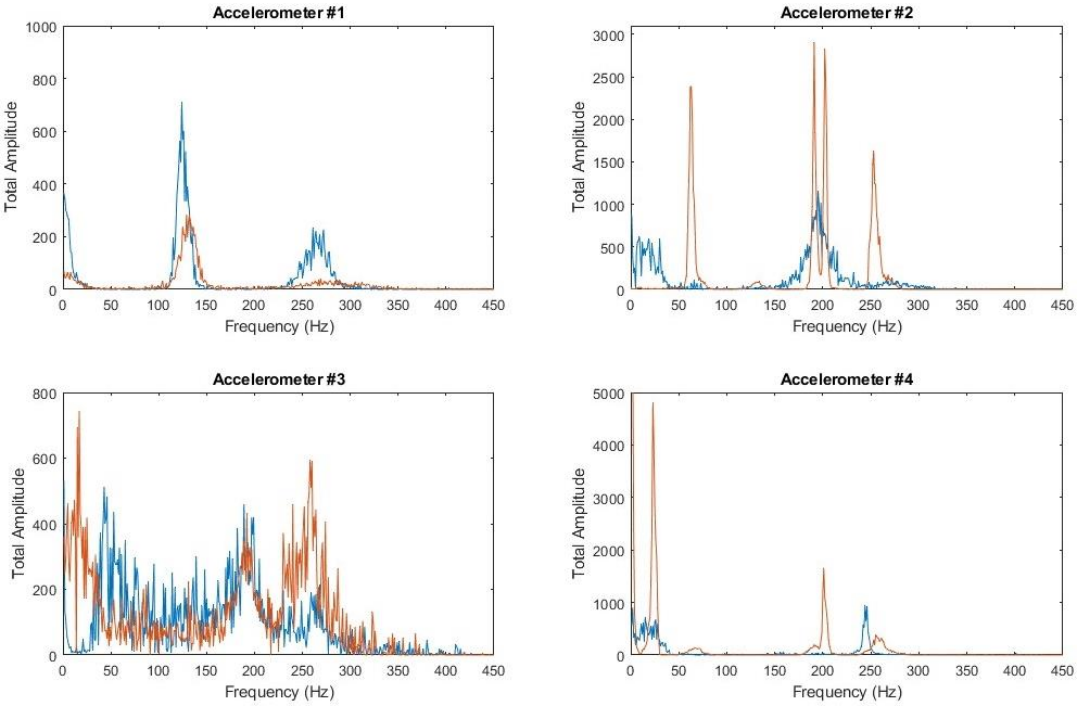

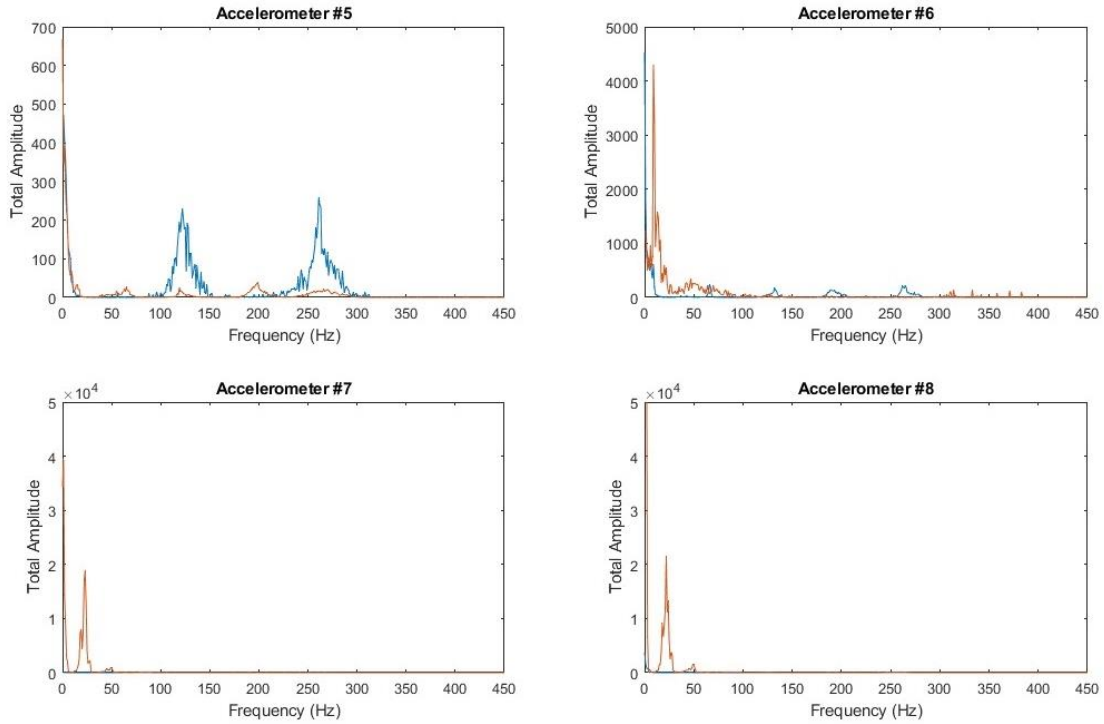

Figure 7. Frequency spectra (Blue for 1.6% moisture content and orange for 7.8% moisture content)

The amplitudes appear to be higher for the sample with a 7.8% moisture content ratio, with the exception found at the locations of accelerometers 1 and 5. The extra moisture caused the sand to flow and interact differently with the tube. The fundamentals of engineering mechanics suggest that the loads exerted on the wall of the tube by the sand changed with the changes to the moisture content ratio causing the frequencies to change. Figure 7 also shows that the dominant frequencies change along the height of the tube. More dominant frequencies are found closer to the top of the tube, where the radial stiffness is less than at the bottom of the tube because the radial stiffness is increased by the clamps (see Figure 4). This suggests that the radial stiffness of the tube effectively damps the radial vibration of the tube.

Acceleration data from three discharges with 150 mm outlet diameter and 1.6% moisture content ratio were analyzed, and the results are shown in Figure 8. The colours blue, orange and yellow – each colour represents the frequency spectrum from each discharge. Despite that all the parameters were kept constant; the dominant frequencies are different across each discharge and at various locations along the height of the tube. The differences in the frequency spectrum inform us that this is a very complex interaction, and there are many influencing parameters that need to be quantified.

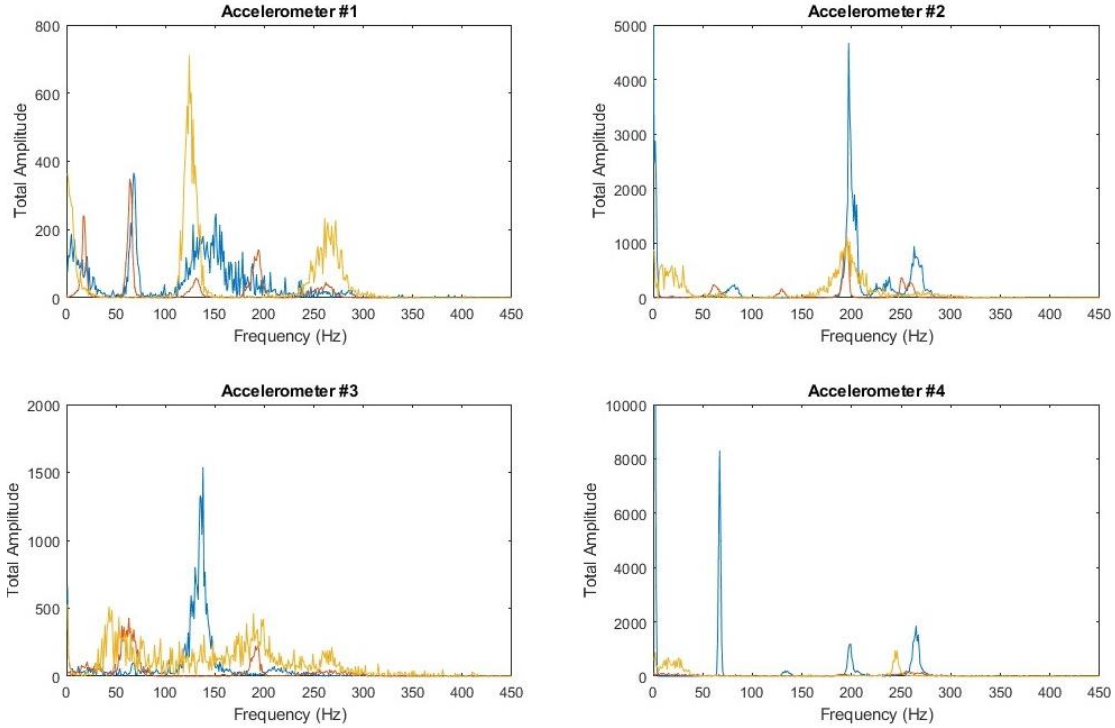

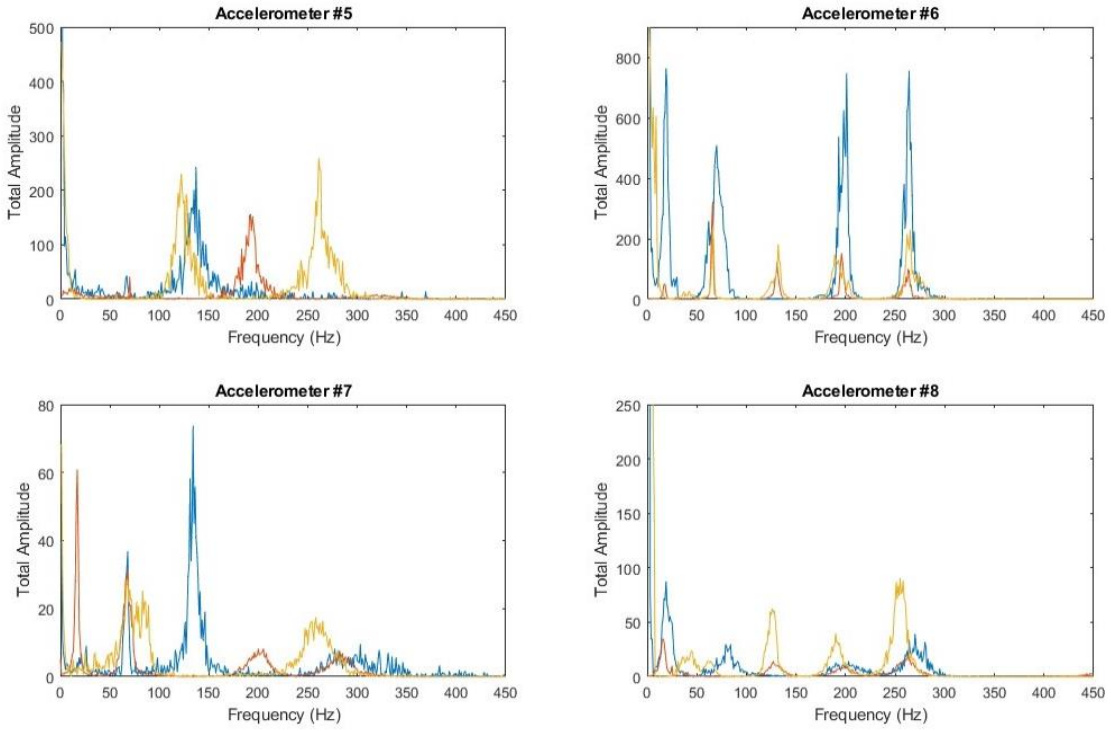

Figure 8. Frequency spectra for 1700 mm fill height, 1.6% moisture content ratio and 150 mm outlet diameter

To our knowledge, the changes to the dominant frequencies along the height of the tube due to the change in the moisture content ratio of the granular material have not been studied. The study of the frequency generated during discharges of this magnitude was first proposed by Tu (2017) [5] and subsequently by Tu et al. (2018) [6] and Tu et al. (2022) [7]. To our understanding, this is because scholars have confined their investigations to the limitations of Janssen's silo load theory, formulated in 1895, and such a theory has been proven to have serious technical shortcomings. The implications of the present findings are as follows:

- The frequency spectrum needs to be further studied and quantified to ensure silos are designed safely because dominant frequencies can lead to resonance and fatigue cracking of welds and members;
- The frequencies generated during discharge need to be incorporated into international design codes; and
- The frequency spectrum can be further developed to enable conditional monitoring of the structural integrity of time varying mass civil engineering structures such as silos and flow conditions automatically without having to shut operation.

4. Conclusions

In this paper, the test data from a series of lab-scale experiments on a silo with sand as the stored material was analyzed and a series of frequency spectra were generated. The natural moisture content of the sand used was 1.6%, and the moisture content was varied by adding water up to 7.8%. Outlet diameters of 60 mm, 90 mm, 120 mm, 150 mm, and 194 mm were selected to vary the discharge rates. Based on this study and the scope of the experimental data, the following conclusions are drawn:

- The frequency spectrum changes and the shape of the frequency spectrum are unrepeatable with each discharge cycle despite keeping all the known influencing parameters constant;
- Each discharge cycle produces different loads despite keeping all known influencing parameters constant;
- The change in the moisture content ratio of the mass inside the storage tube changes the frequency spectrum and dominating frequencies significantly;
- The loads generated during discharge change with the change in the moisture content ratio;
- Different positions along the height of the tube have different dominant frequencies.

The findings outlined in this paper warrant further studies into the interaction between the flowing granular particle and the overall silo structure to quantify the load influencing parameters, such as stiffness of the overall silo, damping of the overall silo, the total mass of the silo, the moisture content ratio of the granular material, particle size distribution,

particle shape, adhesion, cohesion, discharge rate, bulk density, Poisson ratio, elastic modulus, and stiffness of the particle, to enable the time varying mass engineering structure like a silo to be designed safer and more economically. Furthermore, the vibration signals can be used to assess the integrity of the storage structure, optimize its structural performance to reduce capital expenditure in real time, and optimize the flow of the mass to maximize the throughput of the plant.

5. Declarations

5.1. Author Contributions

Conceptualisation, P.T., V.V., and H.C.; methodology, P.T.; software, P.T.; validation, P.T., V.V. and C.H.; formal analysis, P.T.; investigation, P.T.; resources, V.V.; data curation, V.V.; writing—original draft preparation, P.T.; writing—review and editing, V.V. and C.H.; visualisation, V.V.; supervision, V.V.; project administration, C.H.; funding acquisition, V.V. All authors have read and agreed to the published version of the manuscript.

5.2. Data Availability Statement

The data presented in this study are available on reasonable request from the corresponding author. The data are not publicly available due to permissions required from Curtin University to access undergraduate theses.

5.3. Funding

The authors received no financial support for the research, authorship, and/or publication of this article.

5.4. Acknowledgements

We would like to thank J. Griffiths [13] for undertaking the experimental work and making the data available to us for further analysis.

5.5. Conflicts of Interest

The authors declare no conflict of interest.

6. References

[1] Cliff, A., Fullard, L. A., Breard, E. C. P., Dufek, J., & Davies, C. E. (2021). Granular size segregation in silos with and without inserts. Proceedings of the Royal Society A: Mathematical, Physical and Engineering Sciences, 477(2245). doi:10.1098/rspa.2020.0242.

[2] Abdullah, M. S. M., Rahiman, M. H. F., Zakaria, A., Kamarudin, L. M., & Mohamed, L. (2019). A Review on Moisture Measurement Technique in Agricultural Silos. IOP Conference Series: Materials Science and Engineering, 705(1), 12001. doi:10.1088/1757-899X/705/1/012001.

[3] Vimonsatit, V., Tu, P., & Fletcher, J. (2022). A Consideration of the Structural Integrity of Time-Varying Mass Systems. American Concrete Institute, ACI Special Publication, SP-351, 38–53. doi:10.14359/51734673.

[4] Xu, Z., & Liang, P. (2022). Modified lateral pressure formula of shallow and circular silo considering the elasticities of silo wall and storage materials. Scientific Reports, 12(1), 7069. doi:10.1038/s41598-022-11305-6.

[5] Tu, P. (2017). Dynamic Response of Silo Supporting Structure under Pulsating Loads. PhD Thesis, Curtin University, Bentley, Australia.

[6] Tu, P., Vimonsatit, V., & Li, J. (2018). Silo quake response spectrum of iron ore train load out bin. Advanced Powder Technology, 29(11), 2775–2784. doi:10.1016/j.apt.2018.07.026.

[7] Tu, P., Vimonsatit, V., & Hansapinyo, C. Frequency spectrum of engineering structures with time varying masses. Journal of Infrastructure Preservation and Resilience, 3(1), 15. doi:10.1186/s43065-022-00059-0.

[8] AS/NZS1170.4. (2007). Structural design actions Part 4: Earthquake actions. Standards Australia, Sydney, Australia.

[9] AS2304. (2019). Water storage tanks for fire protection systems. Standards Australia, Sydney, Australia.

[10] Asencio, K., Acevedo, M., Zuriguel, I., & Maza, D. (2017). Experimental Study of Ordering of Hard Cubes by Shearing. Physical Review Letters, 119(22), 228002. doi:10.1103/PhysRevLett.119.228002.

[11] Dragomiretskiy, K., & Zosso, D. Variational Mode Decomposition. IEEE Transactions on Signal Processing, 62(3), 531–544. doi:10.1109/TSP.2013.2288675.

[12] Isham, M. F., Leong, M. S., Lim, M. H., & Ahmad, Z. A. Variational mode decomposition: mode determination method for rotating machinery diagnosis. Journal of Vibroengineering, 20(7), 2604–2621. doi:10.21595/jve.2018.19479.

[13] Griffiths, J. (2018). Impact of Moisture Content on the Dynamic Response of a Silo Model Wall during Discharge. Bachelor of Engineering, Curtin University, Bentley, Australia.

[14] AS1289.3.6.1. (2009). Methods of testing soils for engineering purposes - Soil classification tests - Determination of the particle size distribution of a soil – Standard method of analysis by sieving. Standards Australia, Sydney, Australia.

[15] AS1289.2.1.1. (2005). Methods of testing soils for engineering purposes - Soil classification tests - Determination of the moisture content of a soil – Oven drying method. Standards Australia, Sydney, Australia.

Available online at www.CivileJournal.org

Civil Engineering Journal

(E-ISSN: 2476-3055; ISSN: 2676-6957)

Vol. 9, No. 01, January, 2023

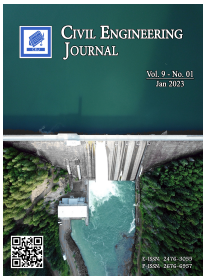

Corrigendum to:

"The Influence of Moisture on the Frequency Spectrum of Time Varying Mass Engineering Structure"

Phung Tu [1*], Vanissorn Vimonsatit [2], Chayanon Hansapinyo [3]

[1] *Flow without Quake, Perth, Western Australia 6000, Australia.*

[2] *School of Engineering, Macquarie University, Sydney, 2113, NSW, Australia.*

[3] *Excellence Center in Infrastructure Technology and Transportation Engineering, Department of Civil Engineering, Chiang Mai University, Chiang Mai, 50200, Thailand.*

Received 14 April 2024; Published 24 April 2024

The current research contains a notation error in Equations 2 to 5. The differential operator $\sigma_v(d_z)$ needs to be $d\sigma_v(z)$. This notation error does not affect other terms in Equations 2 to 5, and in particular does not affect the cancellation of the term $\sigma_v(z)$ going from Equation 2 to Equation 3. The corrected Equations 2 to 5 are shown below with Equation 1 added for completeness.

$$\sigma_v(z) + g\rho_b A dz - \tau_w(z) - \sigma_v(z+dz) = 0 \quad (1)$$

$$\sigma_v(z) + g\rho_b A dz - \tau_w(z) - \sigma_v(z) - d\sigma_v(z) = 0 \quad (2)$$

$$g\rho_b A dz - \tau_w(z) - d\sigma_v(z) = 0 \quad (3)$$

$$g\rho_b A dz = \tau_w(z) + d\sigma_v(z) \quad (4)$$

$$g\rho_b A dz = K\tan(\varphi_x)\sigma_v(z) + d\sigma_v(z) \quad (5)$$

* Corresponding author: phung.tu@flowwithoutquake.com

http://dx.doi.org/10.28991/CEJ-2023-09-01-02